Improved coupled-mode theory for high-index-contrast photonic platforms

Qing Li [1,*] Gregory Moille,[2,3] Hossein Taheri [4] Ali Adibi,[5] and Kartik Srinivasan [2,3]

[1]*Department of Electrical and Computer Engineering, Carnegie Mellon University, Pittsburgh, Pennsylvania 15213, USA*
[2]*Microsystems and Nanotechnology Division, National Institute of Standards and Technology, Gaithersburg, Maryland 20899, USA*
[3]*Joint Quantum Institute, NIST/University of Maryland, College Park, Maryland 20742, USA*
[4]*Department of Electrical and Computer Engineering, University of California at Riverside, Riverside, California 92521, USA*
[5]*School of Electrical and Computer Engineering, Georgia Institute of Technology, Atlanta, Georgia 30332, USA*

(Received 28 August 2020; accepted 16 November 2020; published 4 December 2020)

Coupled-mode theory (CMT) has been widely used in optics and photonics design. Despite its popularity, several different formulations of CMT exist in the literature, and their applicable range is not entirely clear, in particular when it comes to high-index-contrast photonics platforms. Here we propose an improved formulation of CMT and demonstrate its superior performance through numerical simulations that compare CMT-derived quantities with supermode calculations and full wave propagation simulations. In particular, application of the improved CMT to asymmetric waveguides reveals a necessary correction in the conventional phase matching condition for high-index-contrast systems, which could lead to more accurate photonic circuit designs involving asymmetric elements.

DOI: 10.1103/PhysRevA.102.063506

I. INTRODUCTION

Coupled-mode theory (CMT) is a simple yet powerful method which has been widely used in many disciplines of physics and engineering [1,2]. In the field of optics and photonics, CMT has proven to be an indispensable tool for optimizing coupling between various photonic components such as waveguides and resonators, despite the availability of commercial software packages that are capable of performing electromagnetic simulations without approximation [3,4]. This is because a full three-dimensional (3-D) simulation for typical photonic structures still takes a significant amount of computing time and resources. On the other hand, the CMT-based approach only needs the electromagnetic fields from individual components, whose simulation can often be simplified to two dimensions (2-D) by utilizing the inherent geometric symmetry. As a result, CMT provides a significant speedup in the device design and optimization compared to approaches based on full 3-D numerical simulations [5–13].

To illustrate the CMT formulation in the context of coupling between adjacent photonic structures, here we use two coupled waveguides—a system of great practical relevance (e.g., in directional couplers)—as an example. Our methodology is as follows: We first review existing CMT formulations and examine how key quantities produced by these approaches compare against exact supermode calculations. We discuss the physical origin of observed differences in the context of superposition rules that are often the starting point for CMT, but which do not necessarily satisfy electric and magnetic field boundary conditions at interfaces or even the self-consistency of Maxwell's equations themselves (e.g., that the electric and magnetic fields cannot be independently specified). We use this insight to propose an improved CMT formalism that obeys Maxwell's equations and boundary conditions (at least for the dominant field components) and examine how these results compare to both supermode calculations and full wave propagation simulations in the specific case of asymmetric waveguides, where existing CMTs tend to most egregiously fail.

Being a first-order perturbation method, a general two-mode CMT would take the following form [2,14]:

$$\frac{d\mathbf{a}(z)}{dz} = i\mathbf{\Gamma}\mathbf{a}(z), \tag{1}$$

where $\mathbf{a}(z) \equiv [a_1(z)\ a_2(z)]^T$ with $a_j(z)$ representing the normalized power amplitude for the waveguide mode j ($j = 1, 2$) propagating in the z direction. $\mathbf{\Gamma} = [\gamma_{11}\ \gamma_{12}; \gamma_{21}\ \gamma_{22}]$ is a 2×2 matrix with γ_{ij} representing the coupling coefficients between the two waveguide modes ($i, j = 1, 2$). While in some cases it is necessary to extend the above two-mode CMT to include more than one mode from each waveguide [15], which itself is a straightforward process, the two-mode CMT formulation is sufficient for many applications. This is because in a typical coupling scenario, only a limited number of modes from each waveguide would contribute to the coupling process, while the rest of the modes are strongly phase mismatched and therefore can be ignored [2]. In addition, the modes under consideration in Eq. (1) are typically well confined in their respective waveguide geometries, resulting in insignificant coupling to radiation modes which can often be neglected in the first-order approximation. For this reason, the system can be considered as lossless, and the coupling matrix $\mathbf{\Gamma}$ becomes real after proper phase normalization (see discussions below) [4,8].

*qingli2@andrew.cmu.edu

The two eigenvalues of Eq. (1) are found as $\gamma_\pm = (\gamma_{11} + \gamma_{22})/2 \pm \sqrt{(\gamma_{11} - \gamma_{22})^2/4 + \gamma_{12}\gamma_{21}}$ [2]. Combined with appropriate initial conditions at $z = 0$, $a_j(z)$ can then be determined. For instance, for $a_1(0) = 1$ and $a_2(0) = 0$, the maximum power transfer ratio from waveguide 1 to 2 is obtained as [4]

$$T_{21}^{\max} = \frac{|\gamma_{21}|^2}{\left|\left(\frac{\gamma_{11}-\gamma_{22}}{2}\right)^2 + \gamma_{12}\gamma_{21}\right|}. \tag{2}$$

A similar equation can be obtained for $T_{12}^{\max}$ by switching the subscripts in Eq. (2). From these results, we see that if $|\gamma_{11} - \gamma_{22}| \gg \max(|\gamma_{12}|, |\gamma_{21}|)$, the maximum power transfer ratio between the two waveguides is much less than 100%, a scenario commonly depicted as being phase mismatched [4]. On the other hand, if $|\gamma_{11} - \gamma_{22}|$ is comparable or smaller than $\max(|\gamma_{12}|, |\gamma_{21}|)$, efficient power transfer between the two waveguides would occur. In fact, one can identify the exact phase-matching condition as $\gamma_{11} = \gamma_{22}$. In this case, power conservation requires $|\gamma_{21}| = |\gamma_{12}|$. This is because if $|\gamma_{21}| \neq |\gamma_{12}|$ when $\gamma_{11} = \gamma_{22}$, the maximum power transfer ratio from one waveguide to the other ($T_{21}^{\max}$ or $T_{12}^{\max}$) will be larger than 100%, which is clearly unphysical. As a result, we conclude that the maximum power transfer ratio in the phase-matched scenario has to be 100% (assuming there is no loss in the coupling process).

II. MAJOR EXISTING CMT FORMULATIONS

Major existing CMT formulations can be summarized by the following formula [2]:

$$\mathbf{\Gamma} = \frac{\Delta\beta}{2}\begin{bmatrix}1 & 0\\ 0 & -1\end{bmatrix} + \begin{bmatrix}P_{11} & P_{12}\\ P_{21} & P_{22}\end{bmatrix}^{-1}\begin{bmatrix}\kappa_{11} & \kappa_{12}\\ \kappa_{21} & \kappa_{22}\end{bmatrix}, \tag{3}$$

where $\Delta\beta \equiv \beta_1 - \beta_2$ is the intrinsic phase mismatch (β_j is the propagation constant of the waveguide mode j when isolated), and P_{ij} and κ_{ij} are defined as

$$P_{ij} = \frac{1}{4}\iint (\mathbf{e}_i^* \times \mathbf{h}_j + \mathbf{e}_j \times \mathbf{h}_i^*)\cdot \hat{z} dS, \tag{4}$$

$$\kappa_{ij} = \frac{\omega}{4}\iint (\epsilon - \epsilon_j)\mathbf{e}_i^* \cdot \mathbf{e}_j dS, \tag{5}$$

where $\mathbf{e}_j$, $\mathbf{h}_j$, and ϵ_j are the electric field, magnetic field, and permittivity of the waveguide mode j when isolated ($j = 1, 2$), respectively; ϵ denotes the permittivity of the coupled waveguide system (note that ϵ_j and ϵ are assumed to be uniform along z but can have distributions in the x-y plane, which is the waveguide cross section); and $dS \equiv dxdy$ denotes the integration in the waveguide cross section. P_{jj} in Eq. (4) represents the propagating power of waveguide mode j and hence equals one when normalized. In addition, a nonzero P_{12} ($= P_{21}^*$) indicates that the two waveguide modes are not necessarily orthogonal to each other due to field overlap [16]. By properly choosing the relative phase of the two waveguide modes, we can always make P_{12} real. For the rest of the paper, we define a real parameter X to represent this power overlap factor in the CMT formulation ($X = P_{12}$). Finally, κ_{ij} can be understood as a first-order dipole perturbation from the waveguide mode j [$\delta\mathbf{P}_j \equiv (\epsilon - \epsilon_j)\mathbf{e}_j$] to the waveguide mode i ($i, j = 1, 2$) [17]. By adopting the same phase choice for a real P_{12}, κ_{ij} coefficients are all real and hence γ_{ij} will also be real.

The CMT formula described in Eq. (3) was primarily developed in the 1980s by a number of authors (Streifer, Hardy, Haus, and Chuang, among others) [2,16–18]. To show that this theory (hereafter referred to as CMT-X) is consistent with our discussion following Eq. (2), we use the following identity [18] (also see Appendix A):

$$\kappa_{12} - \kappa_{21} = P_{12}\Delta\beta. \tag{6}$$

A straightforward calculation for $\mathbf{\Gamma}$ in Eq. (3) then results in

$$\gamma_{11} - \gamma_{22} = \frac{\gamma_{12} - \gamma_{21}}{X} = \frac{\kappa_{11} - \kappa_{22} + \Delta\beta}{1 - X^2}, \tag{7}$$

showing explicitly that when the phase matching condition is satisfied (i.e., $\gamma_{11} = \gamma_{22}$ for which $\Delta\beta_{\mathrm{PM}}^X = \kappa_{22} - \kappa_{11}$), $\gamma_{12} = \gamma_{21}$. Another widely used CMT formulation, initially developed by Snyder, Yariv, *et al.*, only focuses on the cross-coupling terms (i.e., κ_{12} and κ_{21}), while intentionally neglecting the self-coupling terms (i.e., κ_{11} and κ_{22}) and the power overlap factor between the two waveguide modes (i.e., X) [3,19]. This simple CMT formulation (hereafter referred to as CMT-O) can be obtained from Eq. (3) by forcing $\kappa_{11} = \kappa_{22} = 0$ and $P_{12} = P_{21} = 0$. As a result, the phase matching condition is reduced to $\gamma_{11} - \gamma_{22} = \Delta\beta = 0$, which is commonly used in the weak-coupling regime but is generally different than that predicted by the CMT-X formulation. We want to point out that CMT-O also satisfies power conservation in the phase-matched scenario. This is because when $\Delta\beta_{\mathrm{PM}}^O = 0$, $\gamma_{12}(= \kappa_{12})$ equals $\gamma_{21}(= \kappa_{21})$ according to Eq. (6).

An effective way to examine the accuracy of various CMT formulations is to compare the eigenvalues of Eq. (1) ($\gamma_\pm$) to the exact propagation constants of the coupled system (i.e., the supermode propagation constants denoted as $\beta_\pm$) [20]. We start with a discussion for symmetric waveguides, for which the phase-matching condition of CMT-X and CMT-O is identical and satisfied since $\kappa_{ij} = \kappa_{ji}$ and $\Delta\beta = 0$. For ease of comparison, we define $\delta\beta_{\mathrm{sum}} \equiv (\beta_+ + \beta_- - \beta_1 - \beta_2)/2$ and $\delta\beta_{\mathrm{diff}} \equiv (\beta_+ - \beta_-)/2$. For symmetric waveguides, $\delta\beta_{\mathrm{diff}}$ characterizes the coupling strength while $\delta\beta_{\mathrm{sum}}$ gives rise to additional phase induced by the coupling process [8,21]. Their corresponding variables in the CMT formulation are defined based on the the eigenvalues of Eq. (1) as $\delta\gamma_{\mathrm{sum}} \equiv (\gamma_+ + \gamma_-)/2$ and $\delta\gamma_{\mathrm{diff}} \equiv (\gamma_+ - \gamma_-)/2$. Specifically, CMT-O and CMT-X predict [2]

$$\text{CMT-O}: \delta\gamma_{\mathrm{sum}} = 0, \delta\gamma_{\mathrm{diff}} = \kappa_{12}; \tag{8}$$

$$\text{CMT-X}: \delta\gamma_{\mathrm{sum}} = \frac{\kappa_{11} - X\kappa_{12}}{1 - X^2}, \delta\gamma_{\mathrm{diff}} = \frac{\kappa_{12} - X\kappa_{11}}{1 - X^2}. \tag{9}$$

The results shown in Eqs. (8) and (9) become identical if $|\kappa_{11}| \ll |\kappa_{12}|$ and $|X| \ll 1$. However, neither condition is necessarily satisfied in practice in high-index-contrast waveguides. This can be seen from the numerical example provided in Fig. 1 for 2-D symmetric waveguides, where we define two quantities, $\sigma_{\mathrm{amp}} \equiv (\delta\gamma_{\mathrm{diff}} - \delta\beta_{\mathrm{diff}})/\delta\beta_{\mathrm{diff}}$ and $\sigma_{\mathrm{phase}} \equiv (\delta\gamma_{\mathrm{sum}} - \delta\beta_{\mathrm{sum}})/\delta\beta_{\mathrm{diff}}$, which quantify how the CMT-based estimates related to coupling strength and phase compare with the exact supermode calculations (the latter determined by a finite element method eigenmode solver). While both

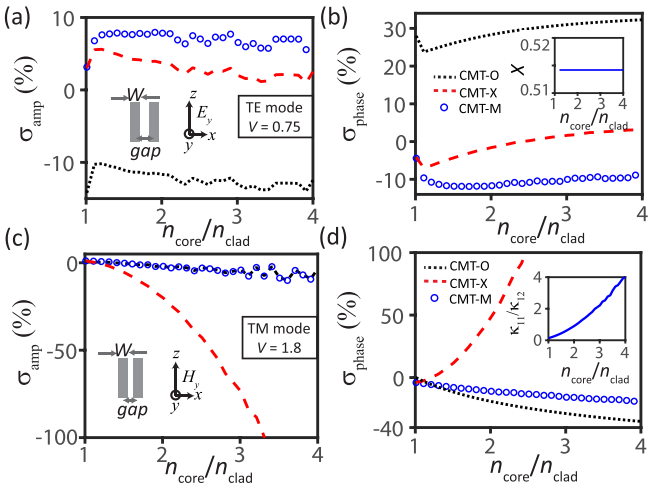

FIG. 1. Numerical comparisons of various CMT formulations for 2-D symmetric waveguides propagating in the z direction: CMT-O (black dotted line), CMT-X (dashed red line), and CMT-M (blue circles). The quantities σ_{amp} and σ_{phase} are defined as $\sigma_{\text{amp}} \equiv (\delta\gamma_{\text{diff}} - \delta\beta_{\text{diff}})/\delta\beta_{\text{diff}}$ and $\sigma_{\text{phase}} \equiv (\delta\gamma_{\text{sum}} - \delta\beta_{\text{sum}})/\delta\beta_{\text{diff}}$, which quantify how the CMT-based estimates related to coupling strength and phase compare with the exact supermode calculations realized using a finite-element method eigenmode solver. [(a), (b)] Transverse-electric (TE) polarization, whose only nonzero electric field component is $\mathbf{E}_y$, for a fixed $V \equiv \pi W\sqrt{n_{\text{core}}^2 - n_{\text{clad}}^2}/\lambda_0 = 0.75$, where $\lambda_0 = 1\ \mu$m is the wavelength, W is the waveguide width, and n_{core} and n_{clad} are the refractive indices of the waveguide core and cladding, respectively. In this example, we choose $gap = W$. The inset in panel (b) plots the power overlap factor in the CMT-X theory ($X = P_{12}$). [(c), (d)] Transverse-magnetic (TM) polarization, whose only nonzero magnetic field component is $\mathbf{H}_y$, for a fixed $V = 1.8$ and $gap = W/3$. The inset in (d) plots the ratio between κ_{11} and κ_{12} defined in Eq. (5). Different values for V are used for the TE and TM polarizations to achieve a similar mode confinement.

formulations perform reasonably well for the transverse-electric (TE) polarization [Figs. 1(a) and 1(b)], where for 2-D waveguides the only electric field component is $\mathbf{E}_y$, the CMT-X formulation is more accurate in the prediction of $\delta\beta_{\text{sum}}$ [Fig. 1(b)]. Note that here the error in estimating $\delta\beta_{\text{sum}}$ through a CMT approach is normalized by the coupling coefficient $\delta\beta_{\text{diff}}$, considering that the induced phase from coupling is a product of $\delta\beta_{\text{sum}}$ and the coupling length L_c, with the latter inversely proportional to $\delta\beta_{\text{diff}}$. The relatively large errors in estimating $\delta\beta_{\text{sum}}$ in the CMT-O approach can be understood by comparing Eq. (8) to Eq. (9): While for the TE polarization the self-coupling term κ_{11} is typically much smaller than κ_{12}, the power overlap factor X may become significant [see the inset of Fig. 1(b)], leading to appreciable errors in $\delta\beta_{\text{sum}}$ if neglected.

In spite of its overall better performance for the TE polarization, the CMT-X formulation produces erroneous results for the TM polarization in high-index-contrast waveguides [22]. One such example is provided in Figs. 1(c) and 1(d), where the errors for both $\delta\beta_{\text{diff}}$ and $\delta\beta_{\text{sum}}$ based on the CMT-X formulation diverge as we increase the refractive index contrast between the waveguide core and cladding (we note that for 2-D waveguides, $\mathbf{H}_y$ is the only magnetic field component for TM polarization). Surprisingly, the CMT-O formulation still works reasonably well despite the lack of justification for ignoring κ_{11} and X. In fact, for the TM polarization the self-coupling term κ_{11} defined in Eq. (5) can be even larger than κ_{12} [see the inset of Fig. 1(d)], resulting in significant errors in the CMT-X formula [Eq. (9)] if κ_{11} is not modeled correctly.

The divergent errors in CMT-X were revealed to stem from the incorrect assumptions made in its derivation [23]. While multiple approaches exist for deriving the CMT-X formula shown in Eq. (3), one invariable assumption is that the transverse electric field [$\mathbf{E}_T(z)$ with "T" denoting the transverse coordinates] and magnetic field [$\mathbf{H}_T(z)$] of the coupled system can be expressed as superposition of individual waveguide modes [2]. That is,

$$\mathbf{E}_T(z) = a_1(z)\mathbf{E}_{1T} + a_2(z)\mathbf{E}_{2T}, \tag{10}$$

$$\mathbf{H}_T(z) = a_1(z)\mathbf{H}_{1T} + a_2(z)\mathbf{H}_{2T}, \tag{11}$$

where $\mathbf{E}_{jT}$ ($\mathbf{H}_{jT}$) denotes the transverse electric (magnetic) field of the individual waveguide mode j ($j = 1, 2$). For the TM polarization in 2-D waveguides, one can easily verify that the assumption for the electric field fails to satisfy the required boundary condition for the $\mathbf{E}_x$ component in Fig. 1(c). Moreover, the two superposition rules specified by Eqs. (10) and (11) are not necessarily compatible with each other, as the electric and magnetic fields are intimately connected through Maxwell's equations and therefore cannot be independently assigned.

III. IMPROVED CMT AND DISCUSSIONS

For the above reason, in this work we only adopt the superposition rule for the magnetic field alone [i.e., $\mathbf{H}(z) = \sum_j a_j(z)\mathbf{H}_j$], for which the required boundary conditions hold for both polarizations. The electric field is then obtained by applying Maxwell's equations, resulting (details in Appendix A) in

$$\begin{aligned}\mathbf{E}(z) &= \frac{i}{\omega\epsilon}\nabla\times\left(\sum_j a_j(z)\mathbf{H}_j\right)\\ &= \sum_j a_j(z)\frac{\epsilon_j}{\epsilon}\mathbf{E}_j + \frac{i}{\omega\epsilon}\frac{da_j(z)}{dz}\hat{z}\times\mathbf{H}_j,\end{aligned} \tag{12}$$

which is different than the assumption made in Eq. (10) for the electric field. With the aid of this result, a corrected version of Eq. (3) for symmetric waveguides is derived as (details in Appendix A):

$$P'_{ij} = \frac{1}{4}\iint\left(\frac{\epsilon_i}{\epsilon}\mathbf{e}_i^*\times\mathbf{h}_j + \frac{\epsilon_j}{\epsilon}\mathbf{e}_j\times\mathbf{h}_i^*\right)\cdot\hat{z}dS, \tag{13}$$

$$\kappa'_{11} = \frac{n_{\text{clad}}^2}{n_{\text{core}}^2}\kappa_{11},\quad \kappa'_{12} = \kappa_{12}. \tag{14}$$

While Eqs. (13) and (14) reduce to Eqs. (4) and (5) respectively for low-index-contrast materials, there are two important corrections for the CMT formulation when the index contrast is large enough. First, Eq. (14) suggests that for the self-coupling term, we should use κ'_{11}, which is significantly smaller than κ_{11} used in the CMT-X theory for

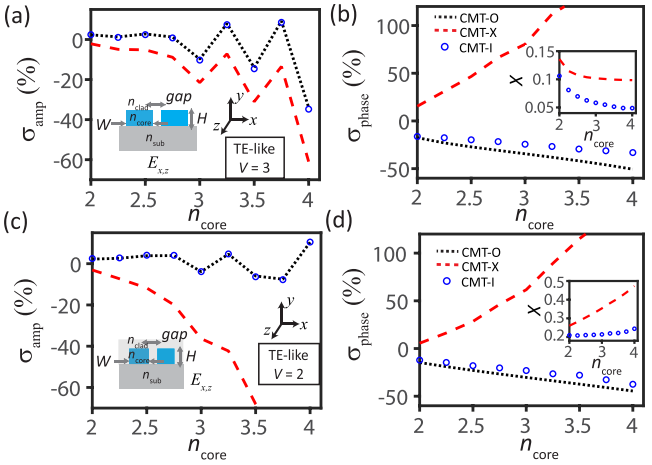

FIG. 2. Numerical comparisons of various CMT formulations for the TE-like polarization (whose dominant electric field components are $\mathbf{E}_x$ and $\mathbf{E}_z$) in 3-D symmetric waveguides (note this TE-like polarization in 3-D corresponds to the TM polarization in 2-D if we reduce the y dimension using the effective index method): CMT-O (black dotted line), CMT-X (dashed red line), and CMT-I (blue circles). $V \equiv \pi W\sqrt{n_{\text{core}}^2 - n_{\text{clad}}^2}/\lambda_0$ with $\lambda_0 = 1$ μm. [(a), (b)] $n_{\text{clad}} = 1$, $n_{\text{sub}} = 1.444$. In this example, we choose $V = 3$, $W/H = 2$, and $gap = W/5$; [(c), (d)] $n_{\text{clad}} = n_{\text{sub}} = 1.444$. In this example, we choose $V = 2$, $W/H = 1.01$, and $gap = W/5$. The insets in panels (b) and (d) plot the power overlap factors in the CMT-X ($X = P_{12}$ for the dashed red line) and CMT-M theories ($X = P'_{12}$ for the blue circles). As in Fig. 1, σ_{amp} and σ_{phase} provided a comparison of the CMT-derived quantities with the exact supermode quantities determined from finite element method simulations.

high-index-contrast waveguides. Second, Eq. (13) indicates that the power overlap factor X should also be modified (P'_{12}), which is numerically smaller than P_{12} used in the CMT-X theory (examples are provided in the inset of Fig. 2). In fact, these two corrections partially justify the assumptions made in the CMT-O formulation regarding κ_{11} and X (both forced to be zero). Numerical results for the TM polarization based on the modified CMT formulation (hereafter referred to as CMT-M), with two examples provided in Figs. 1(c) and 1(d) (blue circles), indeed confirm that it consistently produces more accurate prediction in $\delta\beta_{\text{sum}}$, while yielding essentially the same results as the CMT-O formulation for $\delta\beta_{\text{diff}}$. The application of the CMT-M formulation for the TE polarization, as shown by blue circles in Figs. 1(a) and 1(b), also produces reasonable results which have a slightly worse percentage error than those based on the CMT-X theory.

The failure of the CMT-X theory for the TM polarization in high-index-contrast waveguides and the improved results based on the CMT-M formulation underscores two important principles in the electromagnetic theory: Satisfying the boundary conditions as well as Maxwell's equations. For TM-like modes, the dominant magnetic field is $\mathbf{H}_y$, rendering the magnetic field a natural choice for the superposition rule in the CMT derivation [24]. A close inspection of the CMT-M formulation reveals that the resulting electric field $\mathbf{E}_x$ satisfies the correct boundary conditions though the $\mathbf{E}_z$ component fails to do so (see Appendix A for details). However, since the CMT-M formulation satisfies Maxwell's equations, such errors can be largely suppressed due to the variational principle (which removes errors to the first order) [2]. In contrast, the CMT-X formulation violates Maxwell's equations by assigning the electric and magnetic fields of the coupled system simultaneously for the TM polarization, leading to divergent first-order errors as evidenced in Figs. 1(c) and 1(d). This understanding of CMT also allows us to explain the superior performance of the CMT-X theory for the TE polarization from a different perspective: Given in this case the dominant electric field is $\mathbf{E}_y$ [see Fig. 1(a)], we can apply the superposition rule for the electric field alone [i.e., $\mathbf{E}(z) = \sum_j a_j(z)\mathbf{E}_i$] and derive the magnetic field from Maxwell's equations. Following the exact same procedure, we can show that this approach leads to the CMT-X formulation (see discussions in Appendix A). In this sense, a unified understanding of the CMT-X and CMT-M theories has been developed in this work, with the former based on the superposition rule for the electric field and the latter based on the superposition rule for the magnetic field.

Given the superior performance of the CMT-X and CMT-M formulations in their respective regimes, an improved CMT (termed as CMT-I) can be formulated by combining their unique features (see Appendix A for details):

$$P_{ij}^I = \frac{1}{4}\iint \left(\frac{\epsilon_i}{\epsilon}\mathbf{e}_{ix}^*\mathbf{h}_{jy} - \mathbf{e}_{iy}^*\mathbf{h}_{jx} + \frac{\epsilon_j}{\epsilon}\mathbf{e}_{jx}\mathbf{h}_{iy}^* - \mathbf{e}_{jy}\mathbf{h}_{ix}^*\right)dS, \tag{15}$$

$$\kappa_{ii}^I = \frac{\omega}{4}\iint (\epsilon - \epsilon_i)\left[\frac{\epsilon_i}{\epsilon}\left(|\mathbf{e}_{ix}|^2 + |\mathbf{e}_{iz}|^2\right) + |\mathbf{e}_{iy}|^2\right]dS, \tag{16}$$

$$\kappa_{ij}^I (i \neq j) = \frac{\omega}{4}\iint (\epsilon - \epsilon_j)\left[\mathbf{e}_i^* \cdot \mathbf{e}_j - \frac{\beta_i - \beta_j}{\epsilon\omega}\mathbf{e}_{jx}\mathbf{h}_{iy}^*\right]dS. \tag{17}$$

Numerical simulations carried out for 3D symmetric waveguides in Fig. 2 confirm that this improved CMT indeed provides an overall better performance than the other two, using the quantities σ_{amp} and σ_{phase} that quantify the difference between CMT-derived values and exact supermode simulations. At the same time, the similar performance of the CMT-M and CMT-O formulations in estimating the coupling strength $\delta\beta_{\text{diff}}$ and coupling phase $\delta\beta_{\text{sum}}$ justifies the widespread use of the simple coupled-mode theory (i.e., CMT-O) for high-index-contrast waveguides in certain applications [10]. Table I summarizes the principal differences between the CMT formulations described in this work with more detailed information provided in the Appendix.

So far our discussion has been limited to symmetric waveguides. We now examine these CMT formulations in the context of asymmetric waveguide coupling. In this case, the exact phase matching condition predicted by CMT-X and CMT-I is generally different than that based on CMT-O, whose phase matching condition is simply $\Delta\beta_{\text{PM}}^O = 0$, or $\beta_1 = \beta_2$. To investigate their difference, we carry out numerical simulations based on fully vectorial wave propagation between two asymmetric waveguides. As illustrated in Fig. 3(a), our model comprises two asymmetric waveguides, with a waveguide mode with unit power launched at the lower input [21]. We examine the phase matching condition by varying the upper waveguide width and coupling length and compare the obtained power transfer ratio between the simulation and various CMT formulations. As can be seen in

TABLE I. Comparisons of various CMT formulations with detailed information provided in Appendix B. All the variables have been defined in the main text, except W_{12} for the CMT-M formalism, which is introduced in Appendix A and needed for the case of asymmetric coupling.

Formulations	Power-overlap maxtrix **P**	Coupling matrix **K**	Comments
CMT-X	$\begin{bmatrix} P_{11} & P_{12} \\ P_{21} & P_{22} \end{bmatrix}$	$\begin{bmatrix} \kappa_{11} & \kappa_{12} \\ \kappa_{21} & \kappa_{22} \end{bmatrix}$	Works well for the TE polarization (2D) and TM-like polarization (3D). However, it produces divergent errors for the TM polarization (2D) and TE-like polarization (3D) in high-index-contrast waveguides.
CMT-O	$\begin{bmatrix} P_{11} & 0 \\ 0 & P_{22} \end{bmatrix}$	$\begin{bmatrix} 0 & \kappa_{12} \\ \kappa_{21} & 0 \end{bmatrix}$	Neglecting the self-coupling terms κ_{11} and κ_{22} and the power overlap factor $P_{12}(P_{21})$ works in practice in many cases, though it lacks justification from the existing theories and becomes less accurate as waveguide asymmetry increases.
CMT-M	$\begin{bmatrix} P'_{11} & P'_{12} \\ P'_{21} & P'_{22} \end{bmatrix}$	$\begin{bmatrix} \kappa'_{11} & \kappa_{12} + \Delta\beta(W_{12} - P_{12}) \\ \kappa_{21} - \Delta\beta(W_{12} - P_{12}) & \kappa'_{22} \end{bmatrix}$	This works well for the general case, though its performance is slightly worse than formulation and justifies the use of the CMT-M formulation for high-index-contrast waveguides.
CMT-I	$\begin{bmatrix} P^I_{11} & P^I_{12} \\ P^I_{21} & P^I_{22} \end{bmatrix}$	$\begin{bmatrix} \kappa^I_{11} & \kappa^I_{12} \\ \kappa^I_{21} & \kappa^I_{22} \end{bmatrix}$	This is an mproved CMT combining unique features from CMT-X and CMT-M, which can be considered as a generalized version for both 2D and 3D waveguides.

Fig. 3(b), CMT-O and CMT-I (which is reduced to CMT-M in this 2-D example) predict the phase-matched W_2 to be 340 and 320 nm, respectively. The wave propagation results shown in Fig. 3(c) confirm that CMT-I is more accurate, achieving a maximum power transfer of 98.5% (limited by the scattering loss) for $W_2 = 320$ nm [blue solid line in Fig. 3(c)] while $W_2 = 340$ nm [black dotted line in Fig. 3(c)] based on CMT-O only reaches a peak coupling efficiency of 90%. This example confirms that the phase-matching condition in high-index-contrast materials is not necessarily $\beta_1 = \beta_2$, which may require correction arising from the self-coupling terms in the coupling process. Finally, comparing the simulated maximum transfer ratio from Eq. (2) and plotted as a magenta solid line in Fig. 3(d) for different waveguide widths W_2 (and hence differing values of $(\beta_1 - \beta_2)/\beta_1$) with the results from various CMTs, we find the CMT-I formulation again provides the overall best agreement. It is worth pointing out that the maximum T_{21} predicted by CMT-O and CMT-I can slightly exceed 100% in the phase-mismatched regime, which is an inherent limitation in such coupled-mode formulations [18].

IV. CONCLUSION

In summary, an improved coupled-mode theory was developed for photonics platforms with high index contrast. Moreover, our work provides insight into the applicable range of existing CMT formulations. It theoretically justifies the use of simple coupled-mode theory for high-index-contrast photonic elements under certain circumstances, while revealing a necessary correction in its phase matching condition for the coupling between asymmetric elements. While our discussion in this work is focused on two waveguides, it would be straightforward to extend our theoretical framework to including multiple waveguides or converting it to the time domain for coupling description between waveguides and resonators or that of multiple cavities [4,5,25]. As such, we believe the proposed coupled-mode theory will find a plethora of applications and lead to more accurate designs in various photonics platforms.

ACKNOWLEDGMENTS

G.M. acknowledges support under the Cooperative Research Agreement between the University of Maryland and NIST-PML.

APPENDIX A: DERIVATION OF THE CMT FORMULATIONS

In this section, we provide a detailed derivation of the modified coupled-mode formulation as well as numerical examples to compare its performance with existing CMT formulations.

Our approach follows closely to the one developed by Chuang [18]. For two arbitrary waveguide modes, they should satisfy the following Maxwell's equations [assuming $\exp(i\beta z - i\omega t)$ format]:

$$\nabla \times \mathbf{H}^{(j)} = -i\omega\epsilon^{(j)}\mathbf{E}^{(j)}, \tag{A1}$$

$$\nabla \times \mathbf{E}^{(j)} = i\omega\mu\mathbf{H}^{(j)}, \tag{A2}$$

where the superscript j denotes the mode index ($j = 1, 2$) and $\epsilon^{(j)}$ is the corresponding permittivity (here we focus on the coupling between dielectric waveguides so permeability μ is assumed to be the same). We proceed by multiplying $\mathbf{H}^{(2)*}$ to both sides of Eq. (A2) for $j = 1$ (dot product) and then multiplying $\mathbf{H}^{(1)}$ to the complex conjugate of Eq. (A2) for

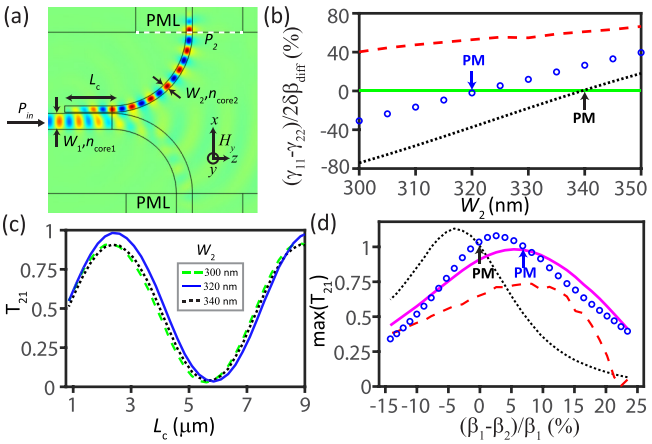

FIG. 3. Numerical comparison of various CMT formulations for the coupling of 2-D asymmetric waveguides for the TM polarization to results from a fully vectorial wave propagation method: for panels (b) and (d), CMT-O (black dotted line), CMT-X (dashed red line), CMT-I (blue circles), and magenta line (wave propagation). (a) Wave propagation simulation: A waveguide mode with unit power is launched from the input of waveguide 1, and the transferred power to waveguide 2 is monitored. Both waveguides are terminated with perfectly matched layers (PMLs), and the overall scattering loss is less than 2%. The phase matching condition is determined by varying the upper waveguide width W_2 and coupling length L_c, with $n_{\text{clad}} = 1, n_{\text{core1}} = 1.8, n_{\text{core2}} = 2.5, W_1 = 800$ nm, $gap = 50$ nm, and $\lambda_0 = 1.55$ μm. (b) Phase matching condition (zero-crossing points) predicted by different CMT formulations. (c) Simulated power transfer ratio T_{21} for different W_2 and L_c based on wave propagation, with the blue solid line ($W_2 = 320$ nm) and the black dotted line ($W_2 = 340$ nm) corresponding to the phase matched condition predicted by the CMT-I theory and the CMT-O theory, respectively. (d) Comparison between the simulated maximum T_{21} for varied W_2 (magenta solid line) and the predictions from various CMT formulations [color scheme same as in panel (b)].

$j = 2$. Adding the resultant two equations together to cancel their right-side term, we obtain the following equation with the aid of Eq. (A1):

$$\frac{d}{dz}\iint \left(\mathbf{E}^{(1)} \times \mathbf{H}^{(2)*} + \mathbf{E}^{(2)*} \times \mathbf{H}^{(1)}\right) \cdot \hat{z} dS = i\omega \iint \left(\epsilon^{(1)} - \epsilon^{(2)}\right)\mathbf{E}^{(1)} \cdot \mathbf{E}^{(2)*} dS. \tag{A3}$$

If we take the two modes as the two waveguide modes under consideration, i.e., $\mathbf{E}^{(1)} = \mathbf{E}_1 \equiv \mathbf{e}_1 \exp(i\beta_1 z)$ ($\epsilon^{(1)} = \epsilon_1$) and $\mathbf{E}^{(2)} = \mathbf{E}_2 \equiv \mathbf{e}_2 \exp(i\beta_2 z)$ ($\epsilon^{(2)} = \epsilon_2$) using the notations in Eqs. (4) and (5) in the main text, we can prove Eq. (6) in a straightforward fashion.

In general, a coupled-mode formulation can be derived based on Eq. (A3) by taking $\mathbf{E}^{(1)}(\mathbf{H}^{(1)})$ as the electromagnetic fields of the coupled system with $\epsilon^{(1)} = \epsilon$ and $\mathbf{E}^{(2)}(\mathbf{H}^{(2)})$ as one of the individual waveguide modes i with $\epsilon^{(2)} = \epsilon_i$ ($i = 1, 2$) [18]. As discussed in the main text, one typical assumption for $\mathbf{E}^{(1)}(\mathbf{H}^{(1)})$, as adopted by Chuang, Haus, *et al.* [2], is that

$$\mathbf{E}_T^{(1)}(z) = a_1(z)\mathbf{E}_{1T} + a_2(z)\mathbf{E}_{2T}, \tag{A4}$$

$$\mathbf{H}_T^{(1)}(z) = a_1(z)\mathbf{H}_{1T} + a_2(z)\mathbf{H}_{2T}. \tag{A5}$$

The z components of EM waves can then be obtained using the other two Maxwell's equations, i.e., $\nabla \cdot \mathbf{D} = 0$ and $\nabla \cdot \mathbf{H} = 0$, resulting in

$$\mathbf{E}_z^{(1)} \approx a_1(z)\frac{\epsilon_1}{\epsilon}\mathbf{E}_{1z} + a_2(z)\frac{\epsilon_2}{\epsilon}\mathbf{E}_{2z}, \tag{A6}$$

$$\mathbf{H}_z^{(1)} \approx a_1(z)\mathbf{H}_{1z} + a_2(z)\mathbf{H}_{2z}. \tag{A7}$$

Substituting Eqs. (A4)–(A7) into Eq. (A3) for $\mathbf{E}^{(1)}(\mathbf{H}^{(1)})$ leads to the CMT-X formulation displayed in Eq. (3) in the main text.

However, there are two major issues with the CMT-X approach for high-index-contrast waveguides: first, the assumption for the transverse electric field could violate the boundary conditions, especially for the TM polarization as discussed in the main text [$\mathbf{E}_x$ component in Fig. 1(c)] [22,23], and second, the assumptions made for the transverse electric and magnetic fields in Eqs. (A4) and (A5) are not necessarily compatible with each other. In fact, one key basis leading to Eq. (A3) is that the electric and magnetic fields must satisfy Eqs. (A1) and (A2) simultaneously, indicating that they are intimately related to each other and therefore cannot be assigned independently.

For the above reasons, here we only use the superposition rule for the magnetic field [i.e., $\mathbf{H}^{(1)}(z) = \sum_j a_j(z)\mathbf{H}_j$] and deduce the electric field following Eq. (A1). A straightforward calculation results in

$$\begin{aligned}\mathbf{E}^{(1)}(z) &= \frac{i}{\omega\epsilon}\nabla \times \left(\sum_j a_j(z)\mathbf{H}_j\right) \\ &= \sum_j a_j(z)\frac{\epsilon_j}{\epsilon}\mathbf{E}_j + \frac{i}{\omega\epsilon}\frac{da_j(z)}{dz}\hat{z} \times \mathbf{H}_j.\end{aligned} \tag{A8}$$

To see the difference of electric field between these two approaches, we use the TM polarization in the 2D case as an example, for which the only nonzero component in the magnetic field is $\mathbf{H}_y$. In this case, Eq. (A8) can be simplified as

$$\mathbf{E}_x^{(1)} = \sum_j a_j(z)\frac{\epsilon_j}{\epsilon}\mathbf{E}_{jx} - \frac{i}{\omega\epsilon}\frac{da_j(z)}{dz}\mathbf{H}_{jy}, \tag{A9}$$

$$\mathbf{E}_z^{(1)} = \sum_j a_j(z)\frac{\epsilon_j}{\epsilon}\mathbf{E}_{jz}. \tag{A10}$$

One immediately sees that $\mathbf{E}_x$ in Eq. (A9) now satisfies the required boundary condition while $\mathbf{E}_x$ in Eq. (A4) fails to do so. On the other hand, the $\mathbf{E}_z$ component given by Eq. (A10) is the same as Eq. (A6), neither of which offers the correct boundary condition for $\mathbf{E}_z$ (which has to be continuous across waveguide boundaries). However, we notice that Eq. (A3) is essentially a quadratic in form with respect to the electric fields, suggesting that it is capable of tolerating their errors to the first order (which is the basis of variational principle) provided that $\mathbf{E}$ and $\mathbf{H}$ satisfy the Maxwell's equations shown in Eqs. (A1) and (A2) [23]. In this sense, the errors in $\mathbf{E}_z$ [Eq. (A10)] can be mitigated to a large extent since we have explicitly satisfied Maxwell's equations through Eq. (A8). By comparison, the CMT-X formulation prioritizes Eqs. (A4) and (A5) over Eqs. (A1) and (A2). As a result, it cannot guarantee the removal of first-order errors originated in the incorrect

boundary conditions, as evidenced in the divergent errors observed in Figs. 1 and 2.

We can now substitute the deduced electric field [Eqs. (A9) and (A10)] into Eq. (A3) for $\mathbf{E}^{(1)}$, along with $\mathbf{E}^{(2)} = \mathbf{E}_i$ and $\mathbf{H}^{(2)} = \mathbf{H}_i$ $(i = 1, 2)$. Using the slow-varying approximation, we only need items up to the first order:

$$\begin{aligned}
&\sum_j \frac{d(a_j e^{i(\beta_j-\beta_i)z})}{dz} \iint \left(\frac{\epsilon_j}{\epsilon}\mathbf{e}_j \times \mathbf{h}_i^* + \mathbf{e}_i^* \times \mathbf{h}_j\right)\cdot \hat{z} dS \\
&\quad - \sum_j \frac{da_j}{dz}\frac{d(e^{i(\beta_j-\beta_i)z})}{dz} \iint \frac{i}{\omega\epsilon}\mathbf{h}_{iT}^* \cdot \mathbf{h}_{jT} dS \\
&= \sum_j a_j e^{(\beta_j-\beta_i)z} i\omega \iint \frac{(\epsilon-\epsilon_i)\epsilon_j}{\epsilon}\mathbf{e}_i^* \cdot \mathbf{e}_j dS \\
&\quad + \sum_j \frac{da_j(z)}{dz} e^{(\beta_j-\beta_i)z} \iint \frac{\epsilon-\epsilon_i}{\epsilon}\mathbf{e}_i^* \times \mathbf{h}_j \cdot \hat{z} dS
\end{aligned} \tag{A11}$$

The above equations can be simplified by defining $\tilde{a}_1(z) \equiv a_1(z)\exp(\Delta\beta z/2)$ and $\tilde{a}_2(z) \equiv a_2(z)\exp(-\Delta\beta z/2)$, with $\Delta\beta \equiv \beta_1 - \beta_2$. We want to point out that the results presented in the main text should be interpreted for $\tilde{a}_j(z)$ (i.e., we have removed the tilde there). With some algebra, we arrive at

$$\begin{aligned}
\frac{d}{dz}\begin{bmatrix}\tilde{a}_1(z)\\ \tilde{a}_2(z)\end{bmatrix} &= i\begin{bmatrix}\frac{\Delta\beta}{2} & 0\\ 0 & -\frac{\Delta\beta}{2}\end{bmatrix}\begin{bmatrix}\tilde{a}_1(z)\\ \tilde{a}_2(z)\end{bmatrix} \\
&\quad + i\begin{bmatrix}P'_{11} & P'_{12}-\Delta\beta H_{12}\\ P'_{21}+\Delta\beta H_{21} & P'_{22}\end{bmatrix}^{-1} \\
&\quad \times \begin{bmatrix}\kappa'_{11} & \kappa'_{12}+\Delta\beta W_{12}\\ \kappa'_{21}-\Delta\beta W_{21} & \kappa'_{22}\end{bmatrix}\begin{bmatrix}\tilde{a}_1(z)\\ \tilde{a}_2(z)\end{bmatrix},
\end{aligned} \tag{A12}$$

where

$$P'_{ij} \equiv \frac{1}{4}\iint \left(\frac{\epsilon_i}{\epsilon}\mathbf{e}_i^* \times \mathbf{h}_j + \frac{\epsilon_j}{\epsilon}\mathbf{e}_j \times \mathbf{h}_i^*\right)\cdot \hat{z} dS, \tag{A13}$$

$$W_{ij} \equiv \frac{1}{4}\iint \left(\frac{\epsilon_j}{\epsilon}\mathbf{e}_j^* \times \mathbf{h}_i + \mathbf{e}_i \times \mathbf{h}_j^*\right)\cdot \hat{z} dS, \tag{A14}$$

$$H_{ij} \equiv \frac{1}{4\omega}\iint \frac{1}{\epsilon}\mathbf{h}_{iT}^* \cdot \mathbf{h}_{jT} dS, \tag{A15}$$

$$\kappa'_{ij} \equiv \frac{\omega}{4}\iint \frac{(\epsilon-\epsilon_i)\epsilon_j}{\epsilon}\mathbf{e}_i^* \cdot \mathbf{e}_j dS. \tag{A16}$$

In Eq. (A12), the term $\Delta\beta H_{12}(\Delta\beta H_{21})$ can be neglected given that both $\Delta\beta$ and $|H_{12}|(|H_{21}|)$ are small. Comparing k'_{ij} defined in Eq. (A16) to κ_{ij} defined in Eq. (5) in the main text, we immediately conclude that

$$\kappa'_{11} = \frac{n_{\text{clad}}^2}{n_{\text{core2}}^2}\kappa_{11},\ \kappa'_{22} = \frac{n_{\text{clad}}^2}{n_{\text{core1}}^2}\kappa_{22}, \tag{A17}$$

$$\kappa'_{12} = \kappa_{21}^*,\ \kappa'_{21} = \kappa_{12}^*. \tag{A18}$$

For symmetric waveguides, the above results are reduced to Eq. (14) in the main text. In the more general case, where $\Delta\beta \neq 0$, we can use Eq. (6) to further simplify Eq. (A12). For example, using the identity $\kappa_{ij} - \kappa_{ji}^* = (\beta_i - \beta_j)P_{ij}$, we obtain

$$\kappa'_{12} + \Delta\beta W_{12} = \kappa_{21}^* + \Delta\beta W_{12} = \kappa_{12} + \Delta\beta(W_{12} - P_{12}), \tag{A19}$$

$$\kappa'_{21} - \Delta\beta W_{21} = \kappa_{12}^* - \Delta\beta W_{21} = \kappa_{21} + \Delta\beta(W_{21} - P_{21}), \tag{A20}$$

while $W_{ij} - P_{ij}$ can be easily calculated based on their definition as

$$W_{ij} - P_{ij} = \frac{1}{4}\iint \frac{\epsilon_j - \epsilon}{\epsilon}\mathbf{e}_j^* \times \mathbf{h}_i \cdot \hat{z} dS. \tag{A21}$$

While the above derivation only relies upon the superposition rule for the magnetic field and therefore in principle should be applicable in the general case, we find in practice it works best for the TM polarization for 2D waveguides (and by extension, the TE-like modes in 3D waveguides). This makes sense considering that the dominant magnetic field for the TM polarization is $\mathbf{H}_y$. On the other hand, for the TE polarization, the dominant electric field is $\mathbf{E}_y$. In this case, we can take the superposition rule for the electric field [i.e., $\mathbf{E}^{(1)} = \sum_j a_j(z)\mathbf{E}_j$], and then derive the magnetic field using Eq. (A2):

$$\begin{aligned}
\mathbf{H}^{(1)} &= \frac{1}{i\omega\mu}\nabla \times \left(\sum_j a_j(z)\mathbf{E}_j\right) \\
&= \sum_j a_j(z)\mathbf{H}_j + \frac{1}{i\omega\mu}\frac{da_j(z)}{dz}\hat{z} \times \mathbf{E}_j.
\end{aligned} \tag{A22}$$

Substituting the obtained $\mathbf{E}^{(1)}$ and $\mathbf{H}^{(1)}$ into Eq. (A3), we find the second term in Eq. (A22) can be neglected since it will produce an expression similar to $\Delta\beta H_{12}$ in Eq. (A12). As a result, we reproduce the result of the CMT-X formulation [Eq. (3) in the main text] from a different perspective. That is, instead of viewing CMT-X as a result of assumptions made in Eqs. (A4) and (A5), it is actually based on the superposition rule for the electric field as well as Maxwell's equations.

Moreover, we want to clarify one common misconception: that the CMT can be further improved by employing the "correct" dipole perturbation based on their boundary conditions [2,23]. For example, in Ref. [23] a correction field was introduced for $\mathbf{E}_x$ in the self-perturbation so that it satisfies the required boundary condition. Mathematically, this means we compute the coupling coefficients κ_{ij} in the following form:

$$\kappa_{ii}^C = \frac{\omega}{4}\iint (\epsilon-\epsilon_i)\left[\frac{\epsilon_i}{\epsilon}|\mathbf{e}_{ix}|^2 + |\mathbf{e}_{iy}|^2 + |\mathbf{e}_{iz}|^2\right] dS, \tag{A23}$$

$$\kappa_{ij}^C (i \neq j) = \frac{\omega}{4}\iint (\epsilon-\epsilon_j)\mathbf{e}_i^* \cdot \mathbf{e}_j dS. \tag{A24}$$

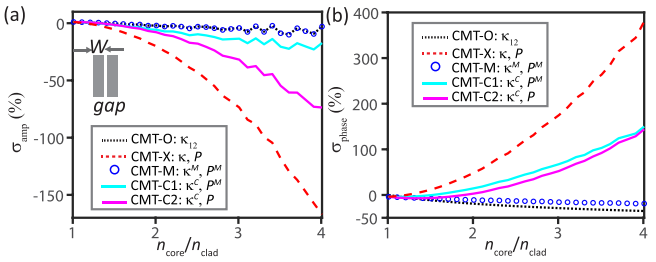

FIG. 4. Extended numerical comparisons of various CMT formulations for the TM polarization in 2-D symmetric waveguides: CMT-O (black dotted line), CMT-X (dashed red line), CMT-M (blue circles), CMT-C1 (cyan line), and CMT-C2 (magenta line). All the simulation parameters are the same as Figs. 1(c) and 1(d), i.e., $V = 1.8$, $gap = W/3$, and $\lambda_0 = 1\ \mu$m.

Using the same example shown in Figs. 1(c) and 1(d) for the TM polarization, we compare this approach (termed as CMT-C) to the CMT-X and CMT-M formulations in Fig. 4. As can be seen, whether we use the P_{ij}^M [Eq. (15)] or P_{ij} [Eq. (4)] coefficients for the CMT-C model (termed as CMT-C1 and CMT-C2, respectively, in Fig. 4), its performance actually is worse than the CMT-M formulation. The answer again lies in the fact that this correction field approach fails to satisfy Maxwell's equations by independently assigning the electric and magnetic fields, thus resulting in first-order errors in the CMT formulation.

APPENDIX B: SUMMARY OF KEY QUANTITIES AND COMPARISON OF CMT FORMULATIONS

In this section, we provide a systematic definition of various CMT formulations used in this work to help the readers track different notations. We start by grouping parameters that are already defined in the text:

(1) intrinsic phase mismatch [see Eq. (3)] $\Delta\beta \equiv \beta_1 - \beta_2$;

(2) conventional power overlap coefficient P_{ij} used by the CMT-X theory [see Eq. (4)],

$$P_{ij} = \frac{1}{4}\iint (\mathbf{e}_i^* \times \mathbf{h}_j + \mathbf{e}_j \times \mathbf{h}_i^*) \cdot \hat{z} dS;$$

(3) conventional coupling coefficient κ_{ij} used by the CMT-O and CMT-X theories [see Eq. (5)],

$$\kappa_{ij} = \frac{\omega}{4}\iint (\epsilon - \epsilon_j)\mathbf{e}_i^* \cdot \mathbf{e}_j dS;$$

(4) modified power overlap coefficient P'_{ij} in the CMT-M theory [see Eqs. (13) and (A13)],

$$P'_{ij} = \frac{1}{4}\iint \left(\frac{\epsilon_i}{\epsilon}\mathbf{e}_i^* \times \mathbf{h}_j + \frac{\epsilon_j}{\epsilon}\mathbf{e}_j \times \mathbf{h}_i^*\right) \cdot \hat{z} dS;$$

(5) modified coupling efficient κ'_{ij} in the CMT-M theory [see Eq. (14) for the symmetric case and Eqs. (A16)–(A18) for the general case],

$$\kappa'_{ij} \equiv \frac{\omega}{4}\iint \frac{(\epsilon - \epsilon_i)\epsilon_j}{\epsilon}\mathbf{e}_i^* \cdot \mathbf{e}_j dS; \tag{B1}$$

(6) auxiliary power overlap coefficient W_{ij} which is a hybrid version of P_{ij} and P'_{ij} [see Eq. (A14)]

$$W_{ij} \equiv \frac{1}{4}\iint \left(\frac{\epsilon_j}{\epsilon}\mathbf{e}_j^* \times \mathbf{h}_i + \mathbf{e}_i \times \mathbf{h}_j^*\right) \cdot \hat{z} dS \tag{B2}$$

[note that W_{ij} and P_{ij} allow us to connect κ_{ij} to κ'_{ij} $(i \neq j)$ through Eqs. (A19) and (A20)];

(7) finally, to take advantage of the superior performance of the CMT-X theory for the TE (2D) polarization and CMT-M theory for the TM (2D) polarization, we have proposed an improved CMT theory by combining their unique features. The new power overlap and coupling coefficients are defined as [see also Eqs. (15)–(17)]:

$$P_{ij}^I = \frac{1}{4}\iint\left(\frac{\epsilon_i}{\epsilon}\mathbf{e}_{ix}^*\mathbf{h}_{jy} - \mathbf{e}_{iy}^*\mathbf{h}_{jx} + \frac{\epsilon_j}{\epsilon}\mathbf{e}_{jx}\mathbf{h}_{iy}^* - \mathbf{e}_{jy}\mathbf{h}_{ix}^*\right)dS,$$

$$\kappa_{ii}^I = \frac{\omega}{4}\iint (\epsilon - \epsilon_i)\left[\frac{\epsilon_i}{\epsilon}(|\mathbf{e}_{ix}|^2 + |\mathbf{e}_{iz}|^2) + |\mathbf{e}_{iy}|^2\right]dS,$$

$$\kappa_{ij}^I (i \neq j) = \frac{\omega}{4}\iint (\epsilon - \epsilon_j)\left[\mathbf{e}_i^* \cdot \mathbf{e}_j - \frac{\beta_i - \beta_j}{\epsilon\omega}\mathbf{e}_{jx}\mathbf{h}_{iy}^*\right]dS.$$

These coefficients are constructed such that they are reduced to the CMT-X and CMT-M formulations for the TE and TM polarizations, respectively.

The various CMT formulations are all given by Eqs. (1) and (3), with different definitions of the power overlap matrix **P** and the coupling coefficient matrix **K** as listed in Table I.

[1] J. R. Pierce, Coupling of modes of propagation, J. Appl. Phys. **25**, 179 (1954).

[2] W. Huang, Coupled-mode theory for optical waveguides: An overview, J. Opt. Soc. Am. A **11**, 963 (1994).

[3] A. Yariv, Coupled-mode theory for guided-wave optics, IEEE J. Quantum Electron. **9**, 919 (1973).

[4] H. A. Haus, *Waves and Fields in Optoelectronics* (Prentice-Hall, New York, 1984).

[5] B. E. Little, S. T. Chu, H. A. Haus, J. Foresi, and J.-P. Laine, Microring resonator channel dropping filters, J. Lightwave Technol. **15**, 998 (1997).

[6] E. S. Hosseini, S. Yegnanarayanan, A. H. Atabaki, M. Soltani, and A. Adibi, Systematic design and fabrication of high-q single-mode pulley-coupled planar silicon nitride microdisk resonator at visible wavelengths, Opt. Express **18**, 2127 (2010).

[7] C. Xiong, W. Pernice, K. K. Ryu, C. Schuck, K. Y. Fong, T. Palacios, and H. X. Tang, Integrated GaN photonic circuits on silicon (100) for second harmonic generation, Opt. Express **19**, 10462 (2011).

[8] M. A. Popovic, C. Manolatou, and M. R. Watts, Coupling-induced resonance frequency shifts in coupled dielectric multi-cavity filters, Opt. Express **14**, 1208 (2006).

[9] M. L. Cooper and S. Mookherjea, Numerically-assisted coupled-mode theory for silicon waveguide couplers and arrayed waveguides, Opt. Express **17**, 1583 (2009).

[10] M. Soltani, S. Yegnanarayanan, Q. Li, and A. Adibi, Systematic engineering of waveguide-resonator coupling for silicon microring/microdisk/racetrack resonators: Theory and experiment, IEEE J. Quantum Electron. **46**, 1158 (2010).

[11] Q. Li, M. Davanco, and K. Srinivasan, Efficient and low-noise single-photon-level frequency conversion interfaces using silicon nanophotonics, Nat. Photon. **10**, 406 (2016).

[12] J. Liu, A. S. Raja, M. Karpov, B. Ghadiani, M. H. P. Pfeiffer, B. Du, N. J. Engelsen, H. Guo, M. Zervas, and T. J. Kippenberg, Ultralow-power chip-based soliton microcombs for photonic integration, Optica **5**, 1347 (2018).

[13] G. Moille, Q. Li, T. C. Briles, S. Yu, T. D. Drake, X. Lu, A. Rao, D. Westly, S. B. Papp, and K. Srinivasan, Broadband resonator-waveguide coupling for efficient extraction of octave-spanning microcombs, Opt. Lett. **44**, 4737 (2019).

[14] D. Marcuse, *Theory of Dielectric Optical Waveguides* (Academic Press, San Diego, 1991).

[15] P. Y. Chen, D. J. Bergman, and Y. Sivan, Generalizing Normal Mode Expansion of Electromagnetic Green's Tensor to Open Systems, Phys. Rev. Appl. **11**, 044018 (2019).

[16] A. Hardy and W. Streifer, Coupled-mode theory of parallel waveguides, IEEE J. Lightwave Technol. **3**, 1135 (1985).

[17] H. A. Haus, W. P. Huang, S. Kawakami, and N. A. Whitaker, Coupled-mode theory of optical waveguides, IEEE J. Lightwave Technol. **LT-5**, 16 (1987).

[18] S. L. Chuang, A coupled-mode theory for multiwaveguide systems satisfying the reciprocity theorem and power conservation, IEEE J. Lightwave Technol. **5**, 174 (1987).

[19] A. W. Snyder, Coupled-mode theory for optical fibers, J. Opt. Soc. Am. A **62**, 1267 (1972).

[20] E. Kapon, J. Katz, and A. Yariv, Supermode analysis of phase-locked arrays of semiconductor lasers, Opt. Lett. **9**, 125 (1984).

[21] Q. Li, M. Soltani, A. H. Atabaki, S. Yegnanarayanan, and A. Adibi, Quantitative modeling of coupling-induced resonance frequency shift in microring resonators, Opt. Express **17**, 23474 (2009).

[22] A. W. Snyder, A. Ankiewicz, and A. Altintas, Fundamental error of recent coupled mode formulations, Electron. Lett. **23**, 1097 (1987).

[23] H. A. Haus, W. P. Huang, and A. W. Snyder, Coupled-mode formulations, Opt. Lett. **14**, 1222 (1989).

[24] L. C. Andreani and D. Gerace, Photonic-crystal slabs with a triangular lattice of triangular holes investigated using a guided-mode expansion method, Phys. Rev. B **73**, 235114 (2006).

[25] S. Fan, W. Suh, and J. D. Joannopoulos, Temporal coupled-mode theory for the Fano resonance in optical resonators, J. Opt. Soc. Am. A **20**, 569 (2003).